

1/06/97

**Nonlinear Electromagnetic Waves and Spherical Arc-Polarized
Waves in Space Plasmas**

Bruce T. Tsurutani
Christian M. Ho
John K. Arballo
Gurbax S. Lakhina
Jet Propulsion Laboratory
4800 Oak Grove Drive
California Institute of Technology
Pasadena, CA 91109

Karl-Heinz Glassmeier
Institut für Geophysik
Technical University of Braunschweig
Mendelssohnstrasse 3, D38106
Braunschweig, Germany

and

Fritz M. Neubauer
Universität zu Köln
Institute für Geophysik und Meteorologie
Albertus-Magnus-Platz
D-5000 Köln 41, Germany

to appear in International Conference on Plasma Physics '96

Abstract

We review observations of nonlinear plasma waves detected by interplanetary spacecraft. For this paper we will focus primarily on the phase-steepened properties of such waves. Plasma waves at comet **Giacobini-Zinner** measured by the International Cometary Explorer (ICE), at comets **Halley** and **Grigg-Skjellerup** measured by Giotto, and interplanetary **Alfvén** waves measured by Ulysses, will be discussed and intercompared. Due to the page limitations of this paper we will keep the cometary wave discussion brief (but references for the interested reader will be provided), and we will focus more on the recent Ulysses observations of phase-steepened **Alfvén** waves. For the latter, classical “interplanetary rotational discontinuities” are explained as phase-steepened edges of **Alfvén** waves. Both the **Alfvén** waves and their phase-steepened edges will be shown to be arc-polarized. A method of determination of the direction of propagation of these waves will be discussed,

INTRODUCTION

The causes of the generation of plasma waves near comets is now well understood (Wu and Davidson, 1972; Thorne and Tsurutani 1987; Lakhina 1987; Tsurutani, 1991; Brinca, 1991; Seeding et al., 1996), The physical picture is quite simple. Comets are “dirty snowballs” that are composed primarily of water ice. As a comet comes close to the sun, the water molecules sublime from the surface of the nucleus and obtain speeds of 1 km s^{-1} relative to the parent body, At 1,0 AU, charge exchange with solar wind protons and photoionization by solar UV photons give a combined lifetime of $\sim 10^6 \text{ s}$ before the neutral molecules (and daughter molecules and atoms: OH and O) are ionized and are picked up by the solar wind, Thus, there is a neutral and an ion cloud with scale of $\sim 10^6 \text{ km}$ surrounding the comet nucleus,

Two extreme cases of the ion pickup process are shown in Figure 1. In the top panel, the magnetic field embedded in the fast flowing solar wind plasma lies in a direction orthogonal to the plasma flow direction, In the bottom panel, the magnetic field is parallel to the solar wind flow, In both cases, the plasma convects the magnetic fields radially outward from the sun. The typical plasma density at 1,0 AU from the sun is $\sim 3-8$ protons cm^{-3} with a temperature of $\sim 1.5 \times 10^5 \text{K}$. The magnetic field magnitude is ~ 5 nT. Thus, the plasma β is $\sim 1,0$ and the Alfvén speed is $\sim 50-70$ km s^{-1} .

In the top panel, the $\vec{V} \times \vec{B}$ Lorentz force will accelerate the freshly created ions and form a ring distribution where the velocity associated with the ring is the solar wind speed, This type of ion distribution is unstable to a left-hand cyclotron resonant instability. In the bottom panel where there is no $\vec{V} \times \vec{B}$ Lorentz force, the ions are stationary in the flowing solar wind plasma and thus comprise a beam flowing at $-\vec{V}_{\text{sw}}$ in the plasma rest frame. This distribution is unstable to the right-hand resonant ion beam instability.

Figure 2 shows the power spectra of the transverse components of the waves at the three comets that have been explored to date: G-Z, Halley and GS. In each of the three cases the peak power occurs close to ~ 10 mHz, the local H_2O ion group cyclotron frequency (the ambient magnetic fields are denoted in each panel). Although the peak power (the pump wave) and the slope of the power at higher frequencies are similar for the three comets, the waveforms are not,

Figure 3a and b shows a comet GZ wave at its initial stage of phase steepening. The three magnetic field components and magnitude are shown in minimum variance coordinates. In this system, the subscripts 1,2 and 3 correspond to the maximum, intermediate and minimum

variance directions, where the wave propagation direction \vec{k} is in the minimum variance direction (Smith and Tsurutani, 1976). Because the magnetic field direction was more or less parallel to \vec{V}_{sw} , the wave is theoretically expected to be right-hand polarized in the plasma frame (from previous arguments).

Several important features should be noted for this wave. Although the “wave period” is ~ 100s, the water group ion cyclotron period, there is little or no phase rotation from the beginning of the interval (shown as “B” at 718:20 UT) to point 1 (719:10 UT). Almost all of the 360° phase rotation of the circularly polarized wave occurs between points 1 and 3. The $B_1 - B_2$ hodogram in Figure 3b illustrates this point. This is what is meant by the authors by “phase-steepening”. The phase rotation is not uniform across the wave, but occurs at one edge. The “wave” is left-hand circularly polarized in the spacecraft frame propagating at -41° relative to \vec{B}_0 . The polarization corresponds to an anomalously Doppler shifted right-hand wave propagating towards the sun, Thus the phase-steepening occurs at the front edge of the wave,

As the comet GZ waves develop further, they become compressive and develop nonlinear whistler packets at their leading edges. This is shown in Figure 4 for a train of these waves. For each wave cycle of ~100s, there is a magnetic compression of $\Delta|B|/B_0 \sim 0.5$ followed in time by a high-frequency (~3s period) whistler packet. Since the wave is propagating in the direction of the sun but is convected past the spacecraft by the high velocity solar wind, the magnetic compression and whistler packets occur at the leading, sunward edges of the waves.

Of the waves at these three comets, those at comet Halley are the most complex (see Tsurutani et al., 1997 and Glassmeier et al., 1997 for an up-to-date discussions). The waves are often without an obviously ordered sense of phase rotation, implying either a superposition of

many waves or a truly “turbulent” state, However, there are times when the waveforms are distinct and somewhat orderly. Figure 5 shows one of these cases. Of the - 100s wave period, the phase rotation occurs in the last -30s, from point 1 to 3. There is little or no rotation from the beginning of the interval to point 1, and then there is a crescent arc-like rotation from points 1 to 2, 2 to 3 and then 3 until the end of the interval. The arc remains in a plane (not shown). More will be said about such polarizations later.

The different types of discontinuities that are possible in a plasma are given in Table 1. For the solar wind, directional discontinuities which involve a rapid rotation of the magnetic field (both rotational and tangential discontinuities are DDs) are the most common, occurring once or twice per hour, shocks less frequent, occurring about once per week, and contact discontinuities the rarest, For rotational discontinuities there is a nonzero mass flux transported across the surface, the change in the magnitudes of the tangential $|\vec{H}|$ component is zero, and the normal field component H_n must be conserved. In short, RDs are sharply kinked Alfvén waves.

Directional discontinuities (DDs) identified by rapid changes in field direction can be either rotational or tangential discontinuities. DDs are identified using computer selection from previously formulated criteria. Two sets of criteria, namely the Tsurutani-Smith (TS) criteria and the Lepping-Behannon (LB) criteria are shown in Table 2. These jump conditions across the discontinuity are applied to 1 minute average magnetic field vectors, Figure 6 shows the magnetic field in RTN coordinates where the TS discontinuities are indicated by the vertical lines. In this coordinate system, \hat{R} points radially away from the sun, \hat{T} is $-\hat{R} \times \hat{\Omega} / |\hat{R} \times \hat{\Omega}|$ where $\hat{\Omega}$ is the solar north polar rotation axis, and \hat{N} completes the right-hand system. Note that there is little or no magnetic field magnitude change occurring across the DDs, Ulysses was 5.2 AU from the sun at a latitude of -6.0° .

Ulysses obtained a gravitational assist from Jupiter to obtain a trajectory that became highly out of the ecliptic. Figure 7 shows the Ulysses trajectory for the post-Jupiter interval and the solar wind parameters during this time. From top to bottom are the solar wind density, magnetic field magnitude, velocity, the occurrence rate of discontinuities detected by the Tsurutani and Smith (1979) and the Lepping-Behannon (1985) methods, the spacecraft radial distance from the Sun and the heliolatitude. Ulysses starts in the ecliptic plane and then goes to -80° latitude.

During this phase (1992- 1994) of the solar cycle, polar coronal holes migrate down to the equator, and high velocity streams emanating from them are detected at ~ 25 day intervals corresponding to the solar rotation period. Such corotating streams are detected in the latter half of 1992 through the first half of 1993, The peak velocity of the streams is ~ 750 to 800 km s^{-1} , whereas the regular solar wind speed is $450\text{-}500 \text{ km s}^{-1}$ (Phillips et al., 1993). What is remarkable about the rate of occurrence of discontinuities during this interval is that the values increase by 5 times when Ulysses is within a high-speed stream and then decreases again as Ulysses comes out of the stream. In the latter half of 1993 through 1994, as Ulysses increased in latitude, it becomes permanently embedded in the coronal stream, The velocity then remains fixed at a value of $\sim 750\text{-}800 \text{ km s}^{-1}$. The occurrence rate of DDs then remained fixed at $\sim 150 \text{ DD day}^{-1}$.

The higher convection speed of the solar wind when Ulysses is within coronal hole streams was studied to determine if this could be the cause of the more frequent detection of DDs. It was found that this mechanism could explain an increase of $\sim 30\%$ in the occurrence rate, far shy of the $\sim 500\%$ increase measured (Tsurutani et al., 1996). Some other explanation had to be found.

Figure 8 shows the return of the magnetic field and plasma velocity when Ulysses was in a high-speed stream. There are large $\Delta\vec{B}/|B|$ -1 to 2 directional fluctuations in the field directionality (and velocity) whereas the field magnitude and velocity remained relatively constant.

To determine the nature of these fluctuations, we examine the cross-correlation between the field and velocity components (see Fig. 9). AU three components have a peak correlation at zero lag and lower values at increasing and decreasing lags. This feature has been interpreted to indicate that the fluctuations are Alfvén waves which are propagating away from the sun.

The relationship between Alfvén waves and discontinuities is shown by one example in Figure 10. There is a slow rotation of the magnetic field directionality from point 1 to 2, A rapid field rotation (the directional discontinuity) occurs from point 2 to 3. The field magnitude is relatively constant across the interval,

The bottom panel gives the rotation of the perturbation vector in the maximum variance (B_1) and intermediate variance (B_2) directions. The Alfvén wave (points 1-2) plus rotational discontinuity (points 2-3) comprise a 360° phase rotation going from point 1 to 2 and then back again (to point 3). The slowly rotating part comprises $\sim 180^\circ$ phase rotation and the RD the other 180° . The entire “wave” can thus be seen to be phase-steepened. The wave is said to be “arc-polarized” (Tsurutani et al., 1994),

The physical meaning of arc-polarized waves is schematically illustrated in Figure 11. A small amplitude linearly polarized wave train is shown in panel a. The perturbation vector is only in the \hat{z} direction, When the wave amplitude increases for noncompressional(Alfvénic) waves, the perturbation vector must rotate on the surface of a sphere (panel b) and thus obtains an “arc”, It should be noted that the wave direction of propagation for these arc-

polarized waves is in the intermediate variance direction ($\hat{\mathbf{B}}_2$) and not in the minimum variance direction as for circularly or elliptically polarized waves as shown in panel c.

Figure 12 gives a statistical summary of the wave direction of propagation relative to the ambient magnetic field for **Alfvén** waves and arc-polarized rotational discontinuities. The bottom panels give the direction of propagation normalized by the solid angle. Both the slowly rotating waves and the RDs propagate nearly along $\vec{\mathbf{B}}_0$.

We have examined the dissipation occurring at these steepened waves (Alfvén shocks) by the plasma (density, temperature, and velocity) and magnetic field jumps across the discontinuities. Figure 13 gives one such analysis. We find little correlation between the temperature and magnetic field jumps, indicating that the dissipation rate is slow relative to the wave dispersion. Other plasma parameters have been analyzed with similar negative results. These observations place constraints on the rate of wave dissipation and at the same time lend confidence to our interpretation that the direction of propagation of these arc-polarized RDs is along the intermediate variance direction.

Acknowledgments. Portions of this research was performed at the Jet Propulsion Laboratory California Institute of Technology, Pasadena under contract with the National Aeronautics and Space Administration, Three of the authors (Bruce Tsurutani, Karl-Heinz Glassmeier and F. M. Neubauer) also wish to thank the Alexander von Humboldt foundation for support for parts of this research. Gurbax S. Lakhina wishes to thank National Research Council for the award of a Senior Resident Research Associateship at the Jet Propulsion Laboratory.

References

Brinca, A., Cometary linear instabilities: From profusion to perspective, in Cometary Plasma Processes, ed. by A. D. Johnstone, Geophys. Mon. 61, AGU, Washington D. C., 211, 1991.

Glassmeier, K.-H., B. T. Tsurutani and F. M. Neubauer, Adventures in parameters of space: A comparison of low-frequency plasma waves at comets, in Nonlinear Waves and Chaos in Space Plasmas, ed. by T. Hada and H. Matsumoto, TERRAPUB, Tokyo, Japan, 1997.

Lakhina, G. S., Low-frequency plasma turbulence during solar wind-comet interaction, Astrophys. Space Sci., 133, 203, 1987.

Lepping, R. P. and K. W. Behannon, Magnetic field directional discontinuities: Characteristics between 0.46 and 1.0 AU, J. Geophys. Res., 91, 8725, 1986.

Phillips, J. L., A. Balogh, S. J. Bame et al., Ulysses at 50° south: Constant immersion in the high-speed solar wind, Geophys. Res. Lett., 21, 1105, 1994.

Seeding, A., K.-H. Glassmeier, S. A. Fuselier, F. M. Neubauer, and B. T. Tsurutani, Comparison of the wave energy transport at comets p/Halley and p/Giacobini-Zinner, Planet. Space Sci., 1996.

Smith, E. J. and B. T. Tsurutani, Magnetosheath lion roars, J. Geophys. Res., 81, 2261, 1976.

Thorne, R. M. and B. T. Tsurutani, Resonant interactions between cometary ions and low-frequency electromagnetic waves, Planet. Space Sci., 35, 1501, 1987.

Tsurutani, B. T. and E. J. Smith, Interplanetary discontinuities: Temporal variations and the radial gradient from 1 to 8.5 AU, J. Geophys. Res., 84, 2273, 1979.

Tsurutani, B. T., C. M. Ho, E. J. Smith, et al., The relationship between interplanetary discontinuities and Alfvén waves: Ulysses observations, Geophys. Res. Lett., 21, 2267, 1994,

Tsurutani, B. T., C. M. Ho, J. K. Arballo, et al., Interplanetary discontinuities and Alfvén waves at high heliographic latitude: Ulysses, J. Geophys. Res., 101, 11027, 1996.

Tsurutani, B. T., K.-H. Glassmeier and F. M. Neubauer, A review of nonlinear low frequency (LF) wave observations in space plasmas: On the development of plasma turbulence, in Nonlinear Waves and Chaos in Space Plasmas ed. by T. Hada and H. Matsumoto, TERRAPUB, Tokyo, Japan 1997,

Wu, C. S. and R. C. Davidson, Electromagnetic instabilities produced by neutral-particle ionization in interplanetary space, J. Geophys. Res., 77, 5399, 1972.

Table Captions

Table 1, Different types of fluid discontinuities which are possible in interplanetary space. In the ecliptic plane and in slow streams, the most frequently types of discontinuities occurring in the solar wind are rotational and tangential discontinuities. Together, these occur at a rate of 1 to 2 per hour.

Table 2, Identification Criteria for Directional Discontinuities (DDs).

Figure Captions

Figure 1. The cometary ion pickup process and free energy associated with plasma wave generation,

Figure 2, Transverse magnetic wave power spectra (orthogonal to the average field direction) for comets: GZ, Halley and GS.

Figure 3. A phase steepened GZ magnetosonic wave. Almost all of the phase rotation of the anomalously Doppler shifted right-hand circularly polarized wave occurs from points 1 to 4 (about 12s), whereas the wave period is - 100s.

Figure 4, More fully developed GZ waves. The waves are compressive $\Delta|B|/B_0$ -0.5, and have nonlinear whistler packets at the leading (antisunward) edges.

Figure 5, A phase steepened Halley wave. Almost all of the wave phase rotation occurs at the leading 1/3 of the wave. The wave is arc-polarized,

Figure 6. Directional discontinuities identified by the TS criteria (at the vertical lines).

Figure 7. The post-Jovian encounter Ulysses plasma and field data, The rate of occurrence of directional discontinuities is highest in high-speed coronal hole streams,

Figure 8. The highly variable field and plasma velocity components in the coronal hole solar wind stream,

Figure 9. Cross-correlation between magnetic field and velocity vector components. Large, positive correlation coefficients at zero lag imply that the fluctuations are due to Alfvén waves. The sense of the wave propagation is outward from the sun,

Figure 10. The relationship between a rotational discontinuity (between points 2 and 3) and a slowly rotating Alfvén wave (points 1 and 2). The rotational discontinuity is the phase-steeped edge of the Alfvén wave. The wave is arc-polarized and to first order noncompressive.

Figure 11, An example of a linearly polarized small amplitude Alfvén wave (a), a large amplitude arc-polarized wave (b), and a circularly or elliptically polarized plane wave (c), For the case (c), the direction of propagation is along the minimum variance direction, which is the same as the direction of \mathbf{B}_0 .

Figure 12. The wave direction of propagation for Alfvén waves (left-hand side) and for arc-polarized RDs (right-hand side).

Figure 13, The relationship between proton temperature and magnetic field magnitude jumps across arc-polarized discontinuities. There is no obvious correlation between the two parameters indicating a lack of obvious dissipation.

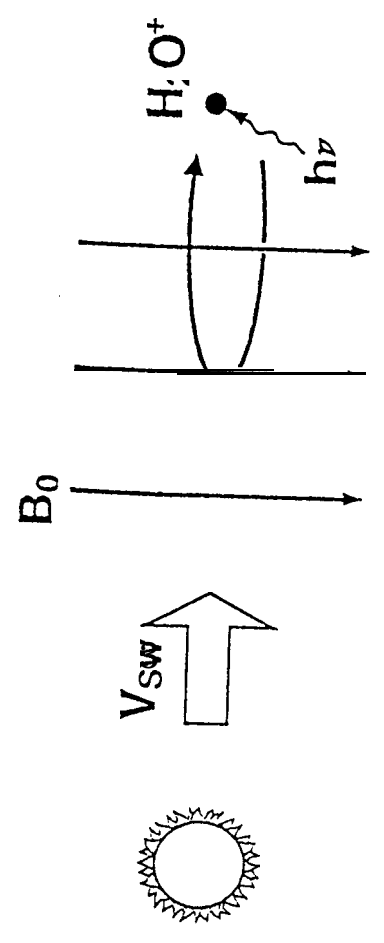
| | MASS FLUX | CHANGE IN MAGNETIC FIELD | |
|--------------------------|------------|--|--------------|
| TYPE OF DISCONTINUITY | ρv_n | $[\vec{H}]$ | |
| CONTACT DISCONTINUITY | 0 | $[\vec{H}_t] = 0$ | $H_n \neq 0$ |
| TANGENTIAL DISCONTINUITY | 0 | $[\vec{H}_t] \neq 0$ | $H_n = 0$ |
| ROTATIONAL DISCONTINUITY | $\neq 0$ | $[H_t] = 0$ | $H_n \neq 0$ |
| SHOCK | $\neq 0$ | $[\vec{H}_t] \neq 0$ $[H_t] \neq 0$ | $H_n \neq 0$ |

Table 1

Table 2. Identification Criteria for Directional Discontinuities (DD)

| Tsurutani-Smith Criteria | Lepping-Behannon Criteria |
|--|--|
| <p>The magnitude of the vector change across the discontinuity 1) must equal or exceed one half the larger of the field magnitudes on either side of the discontinuity (i.e., $\Delta\mathbf{B} / \mathbf{B} > 0.5$).</p> <p>2) The vector jump across the discontinuity must be large in comparison with the general level of vector fluctuations on either side of the discontinuity (i.e., $\Delta\mathbf{B} \geq 2\delta$, where δ is the value of the field variance on either side of the DD).</p> <p>3) Adjacent discontinuities must be separated by 3 or more minutes.</p> | <p>The angular change between successive 42 s averages (however, we use 1 min averages) must be ≥ 30 degrees.</p> <p>2) Data gaps within 2 data points before or 2 points after the discontinuity are not permitted (i.e., the data adjacent to the [discontinuity must be continuous). A detected discontinuity is rejected if gaps are found.</p> <p>3) DDs for which the vector change between either 2 points before or 2 points after the DD is > 45 degrees are rejected. This disallows interpreting large smooth changes as discontinuities.</p> <p>4) The angular change in the field calculated from the average of the two points before the DD and the two points after must also equal or exceed 30 degrees.</p> <p>5) Two successive DDs satisfying the above criteria are permitted (the two are counted as a single discontinuity, the one with the largest angular change {(1) above} being reported as the discontinuity), but any other DD occurring within 4 points before or 4 points after causes the rejection of both. This test rejects step-step or box-like structures.</p> |

a



b

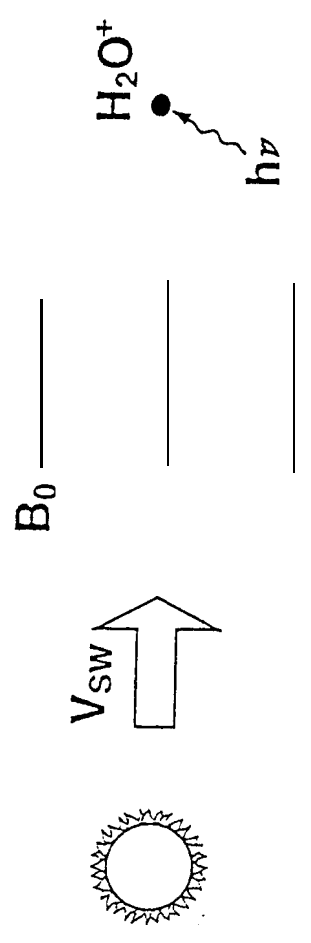
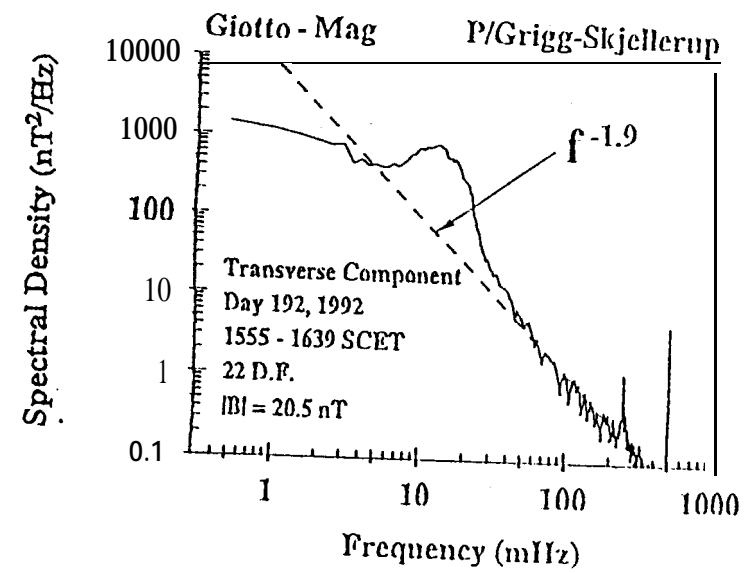
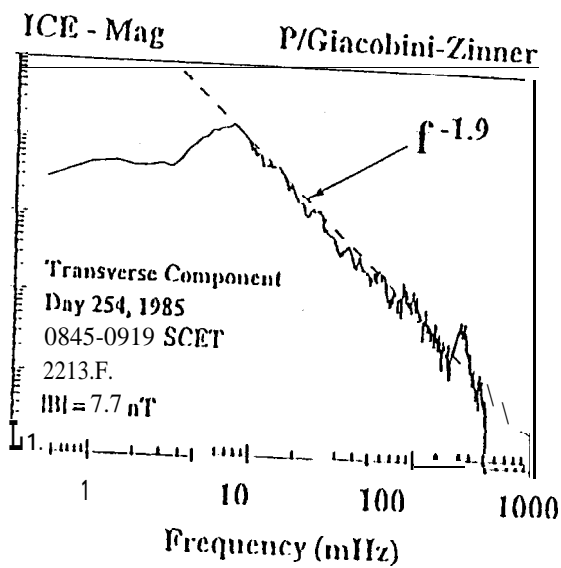


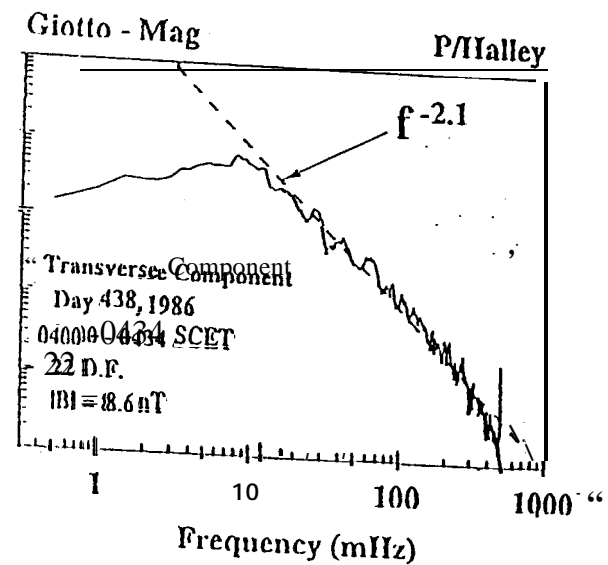
Figure 1



a)



b)

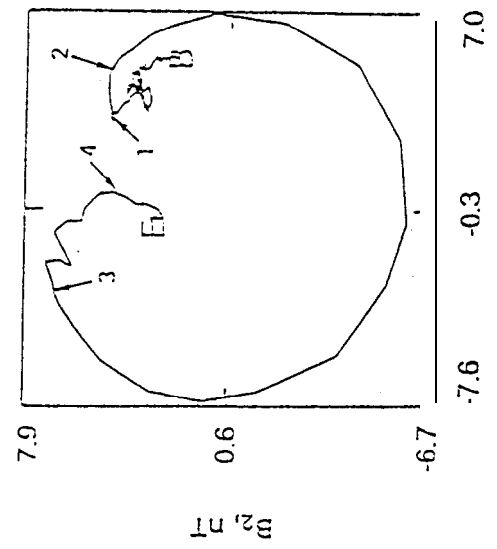
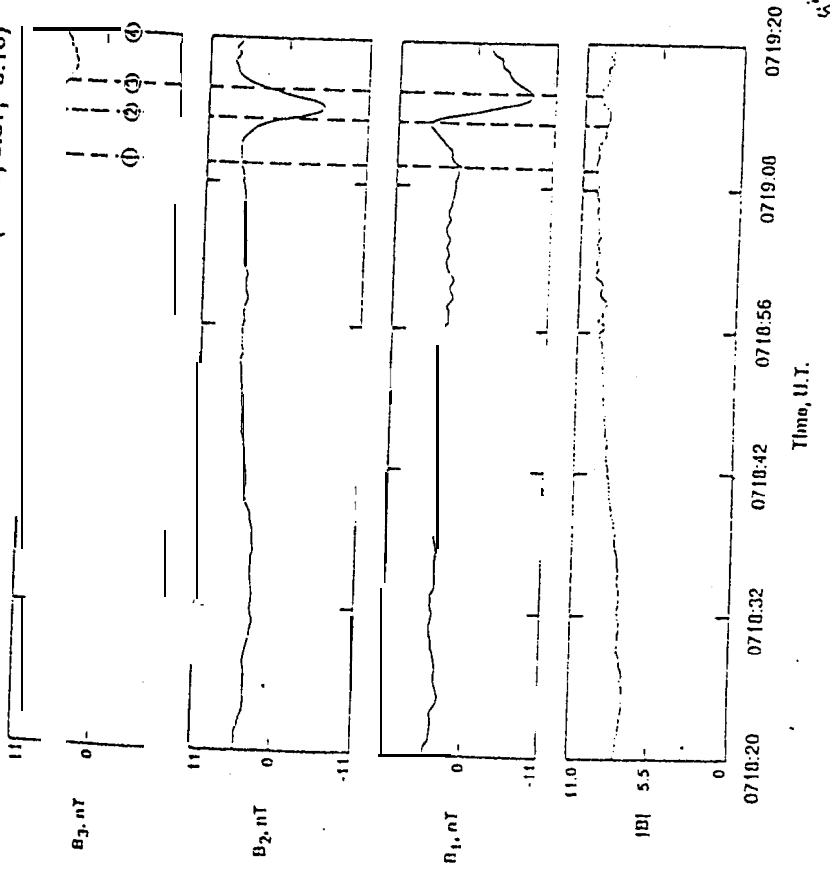


c)

Figure 2

1985, Day 254
 0718:20 - 0719:20 U.T.

$u_{k0} = 11$
 $\lambda_1/\lambda_2 = 2.1$
 $\lambda_2/\lambda_3 = 3.2$
 $\tilde{n} = (-0.80, 0.57, -0.18)$



Figures 3a, b

ICE at Comet Giacobini-Zinner

September 11, 1985
Day 254

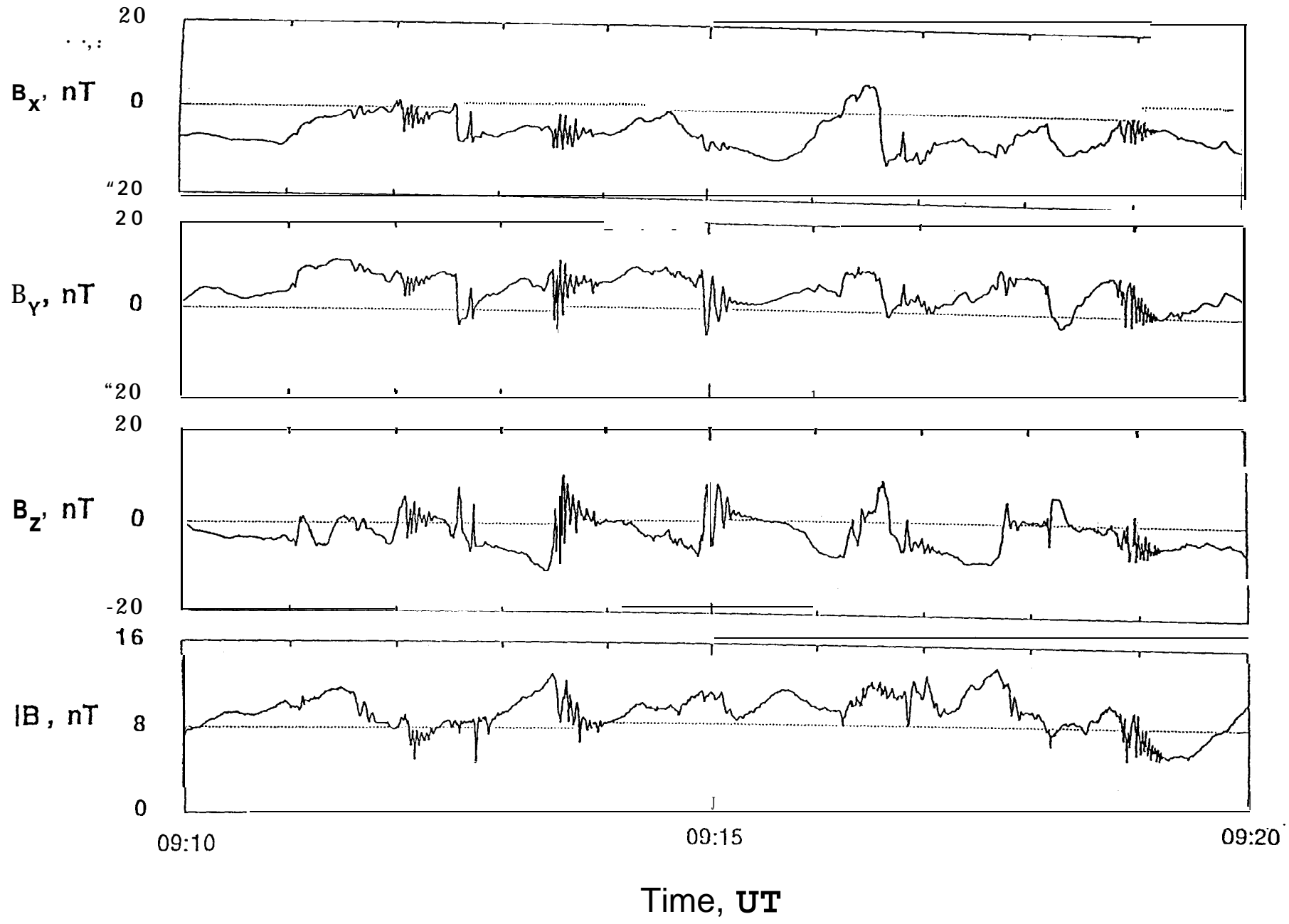
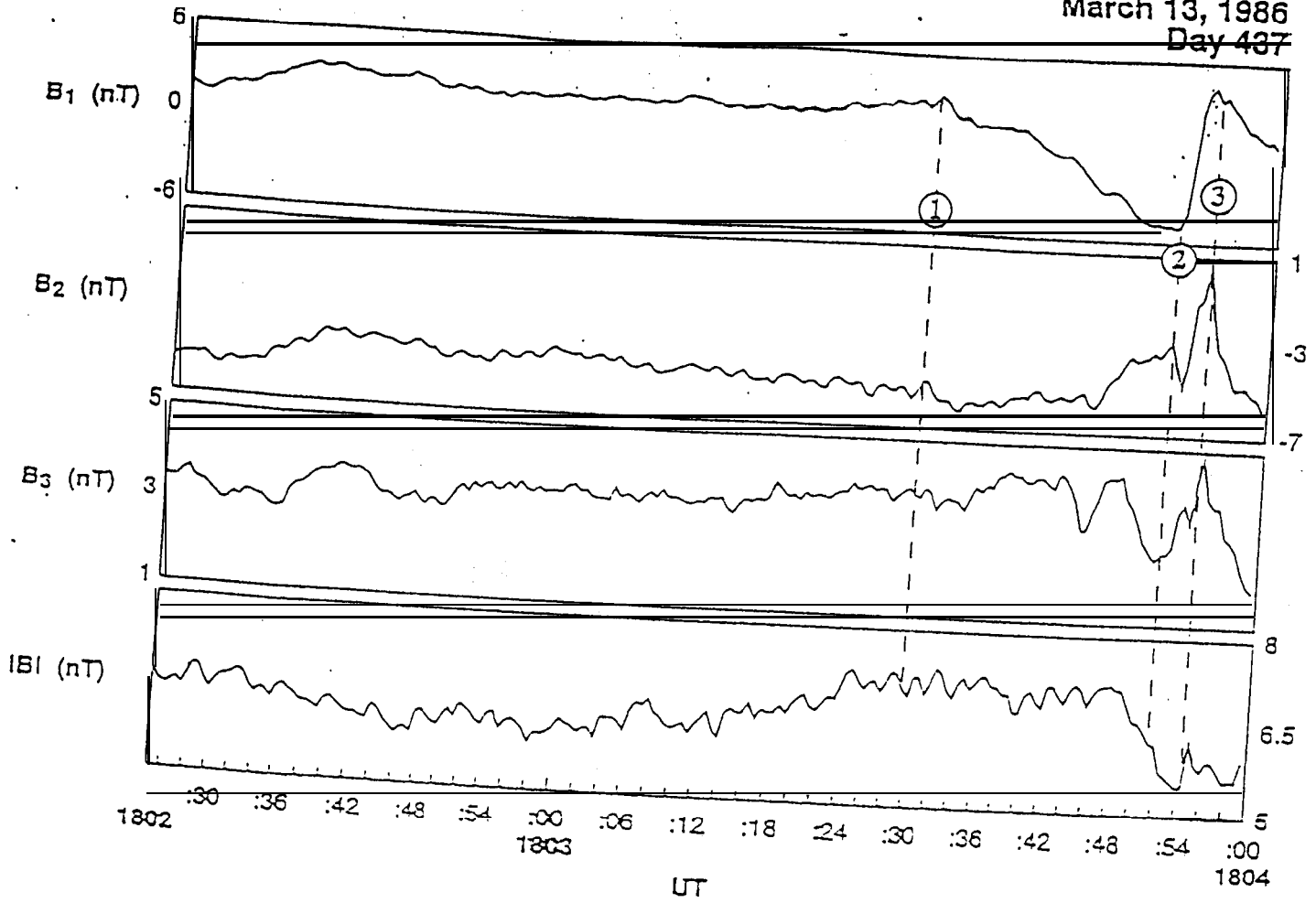


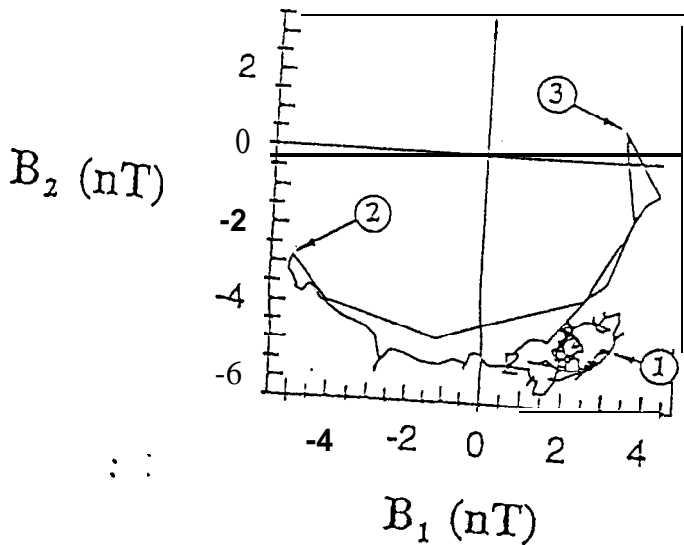
Figure 4

Giotto

March 13, 1986
Day 437



Day 437
1802:25-1804:00 UT



$$\lambda_1/\lambda_2 = 4.98 \quad \lambda_2/\lambda_3 = 4.02$$

$$ev(3) = (-0.625, 0.763, -0.162)$$

$$\langle B \rangle = (-4, 8, 3.5)$$

$$\theta_w = 54.60^\circ \quad Res.: 0.500 \text{ aver.}$$

Ulysses Magnetic Field Data R=5.22AU, Lat=-6.0, Long=175.1

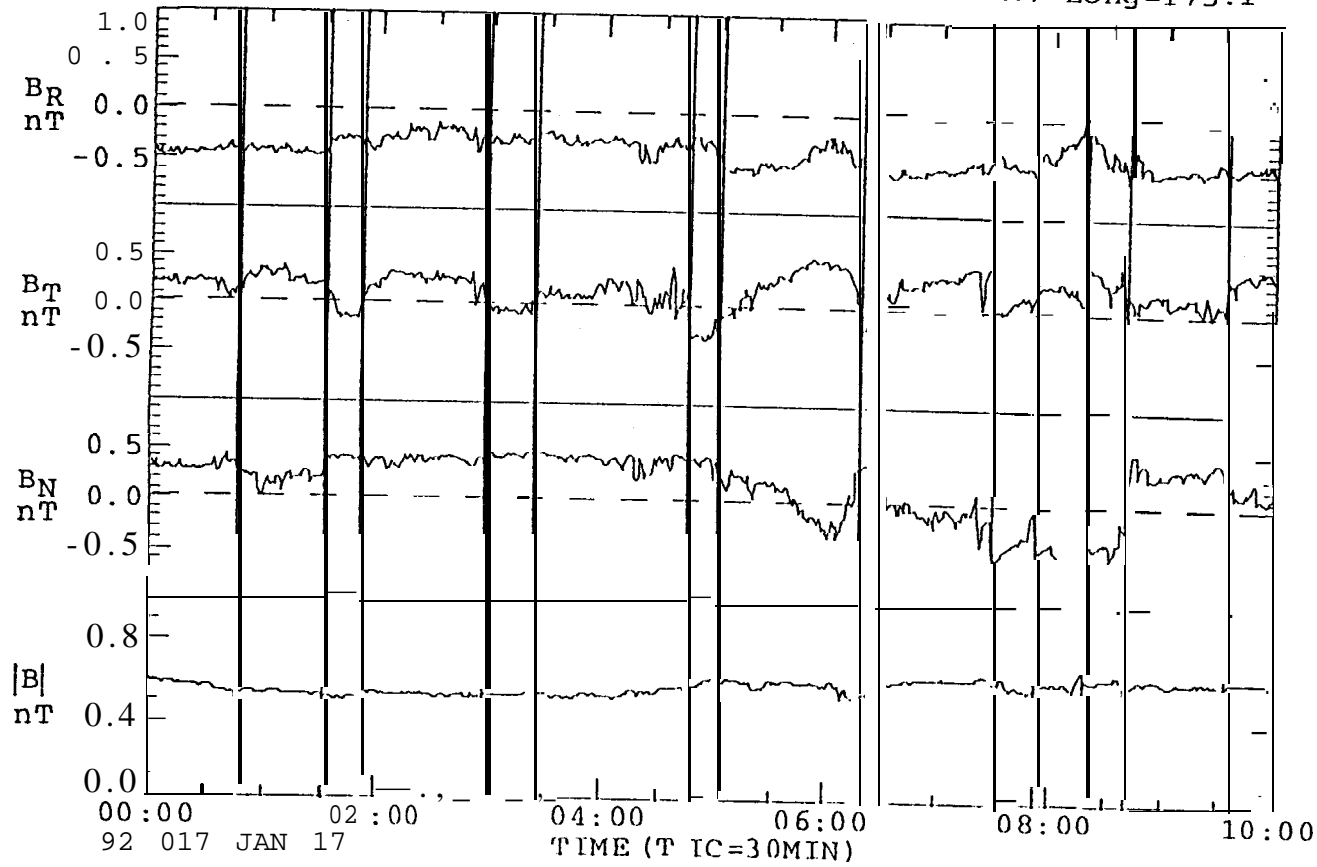


Figure 6

Ulysses out of the ecliptic plane after the Jupiter encounter

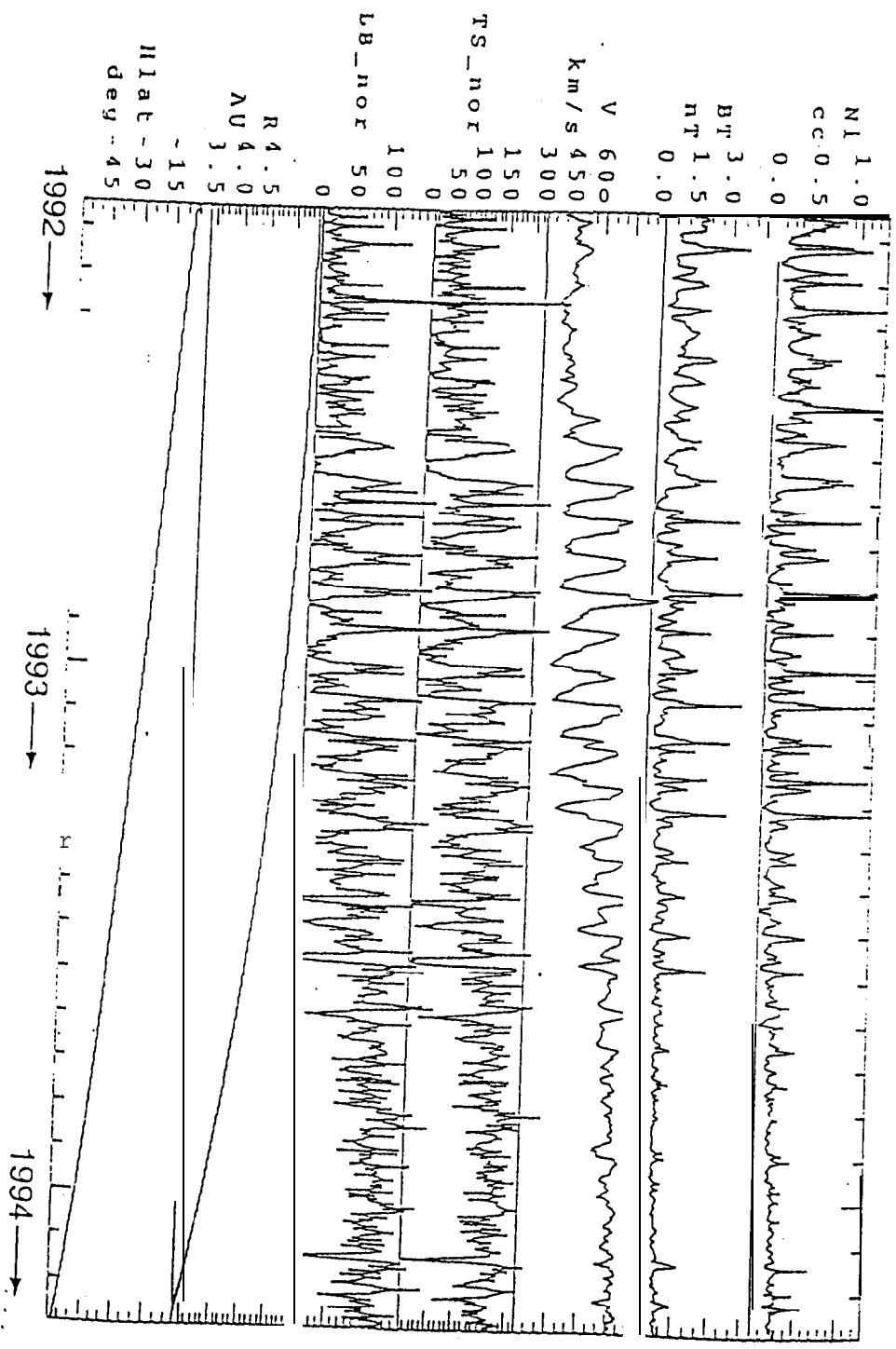


Figure 7

Time, CT.

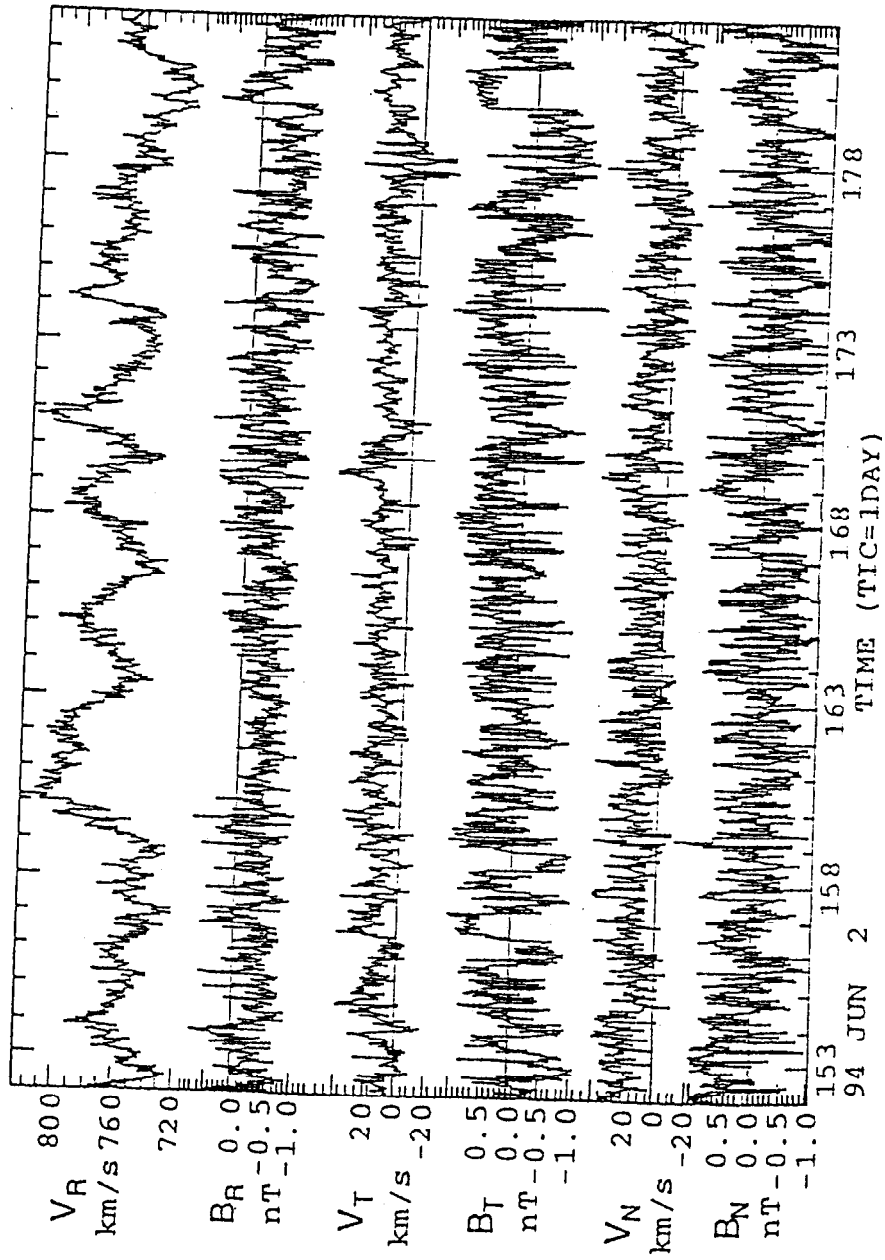
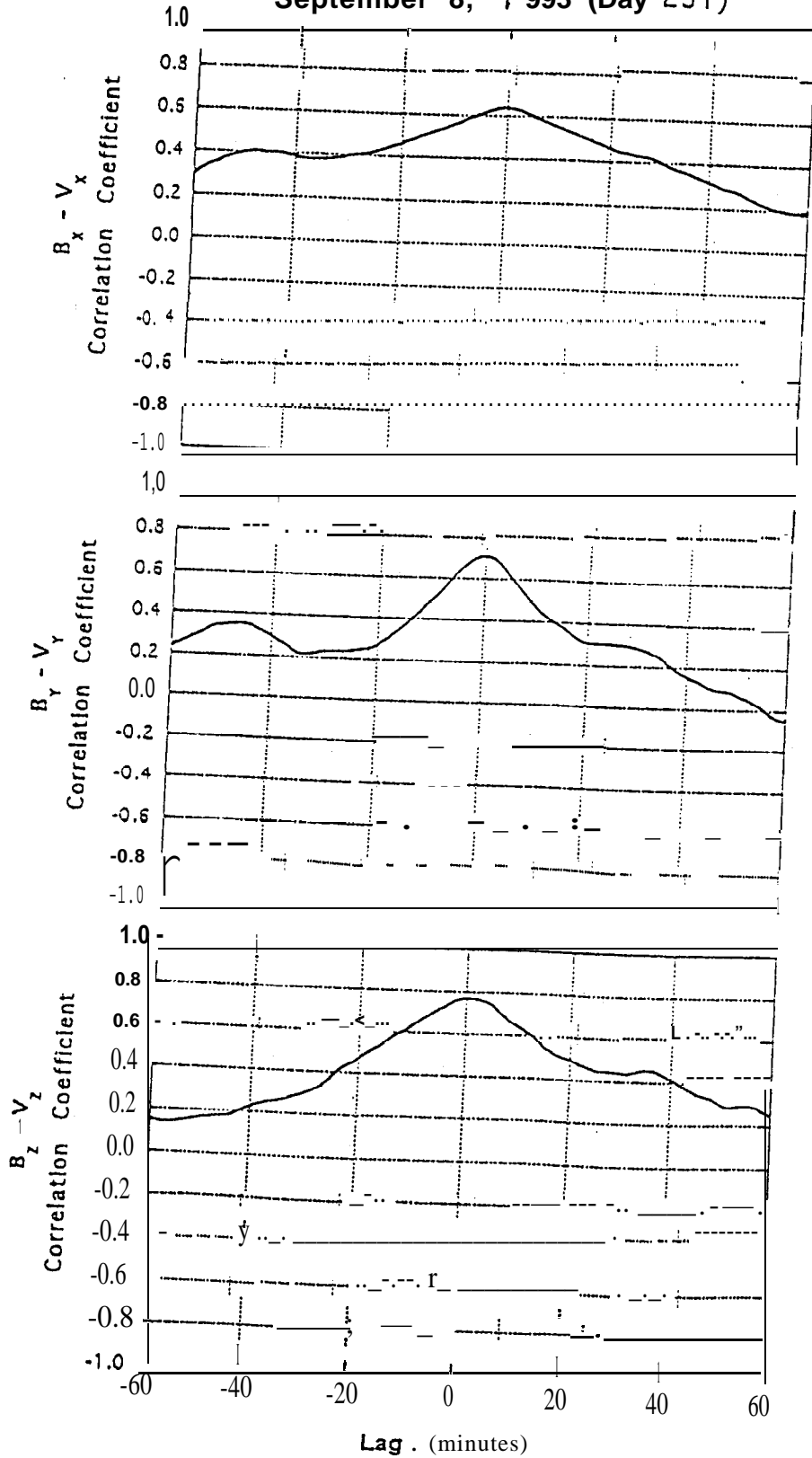


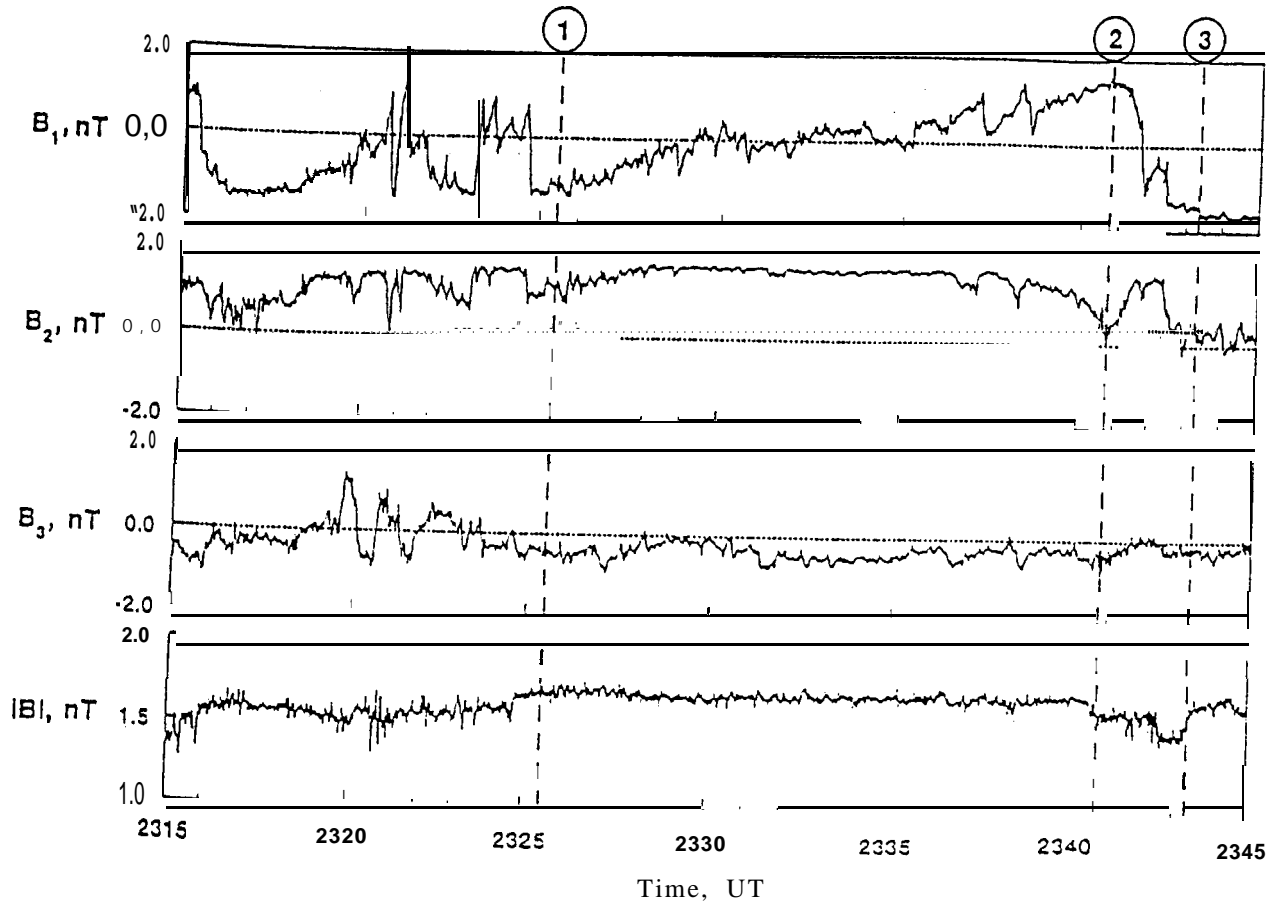
Figure 8

Ulysses
September 8, 1993 (Day 251)

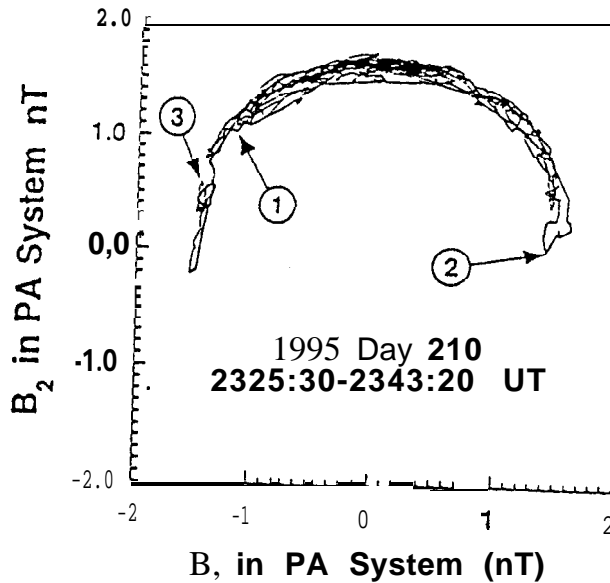


Ulysses

July 29, 1995
Day 210



Ulysses Heliographic Latitude $\approx 80.2^\circ$



- ① 2325:31 UT
- ② 2340:47 UT
- ③ 2343:20 UT

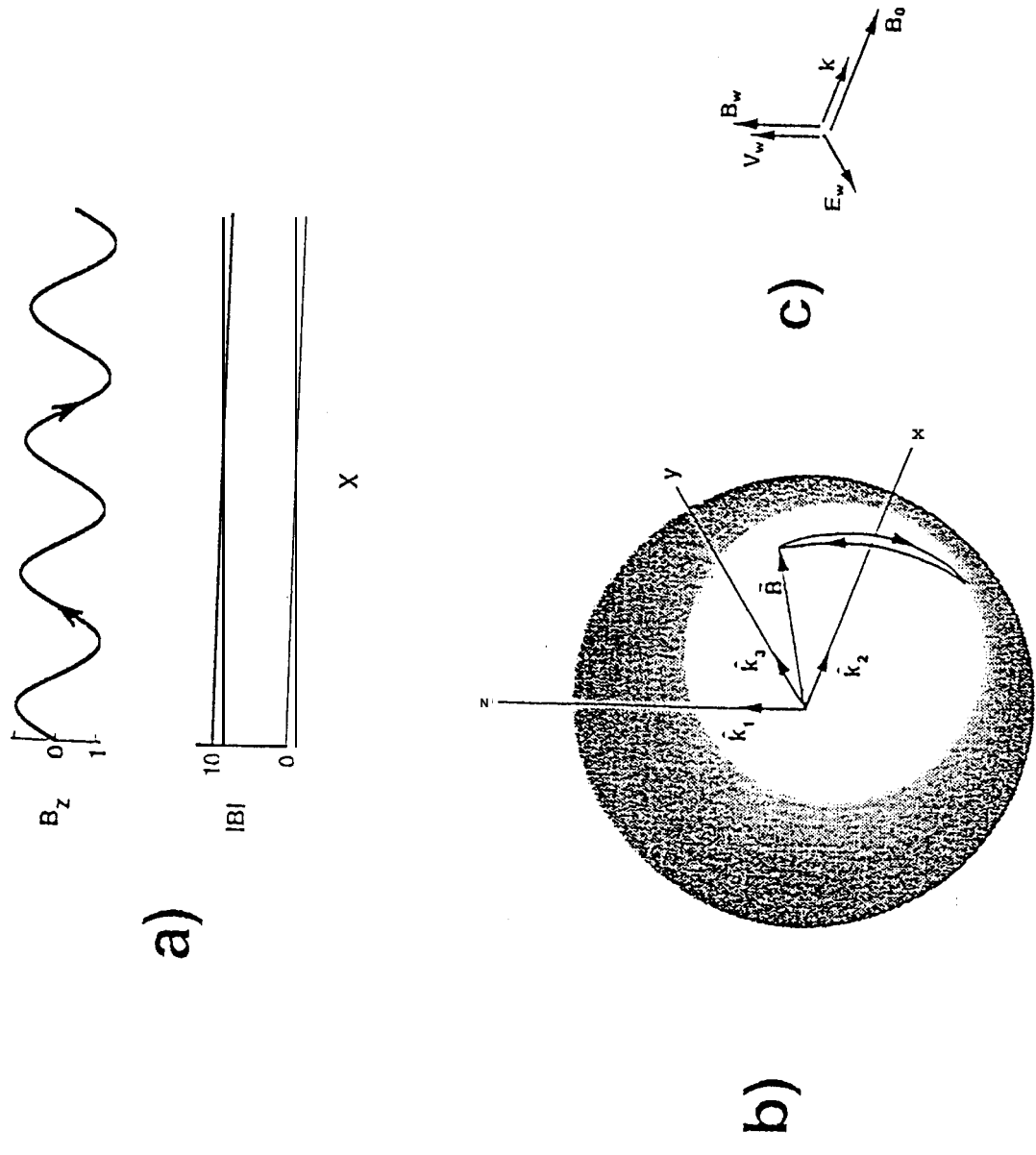
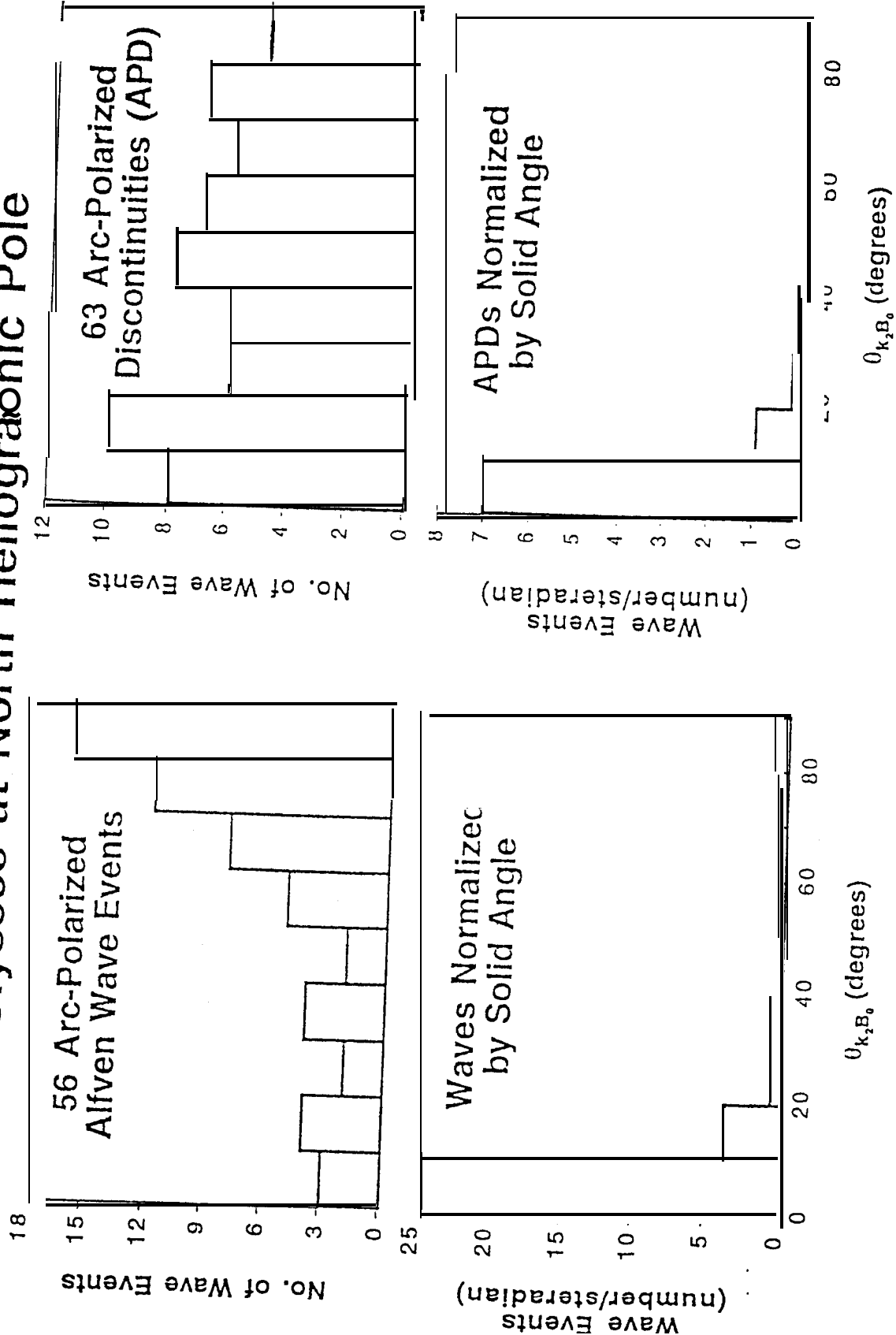


Figure 11

Ulysses at North Heliographic Pole



Ulysses Arc-Polarized RD
95 218

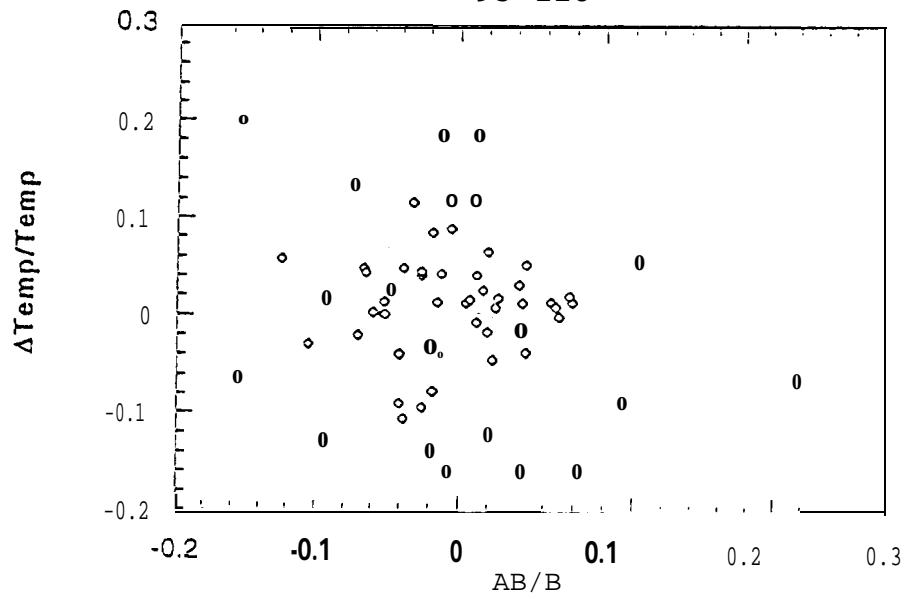


Figure 13